International Journal of Recent Technology and Engineering (IJRTE)
ISSN: 2277-3878 (Online), Volume-8 Issue-4, November 2019

Simulation of Impeller Exit Flows of A Centrifugal Blower

Seralathan S, Balaji R, Mukesh Nadarajan, Ijas Ahamed A, Hariram V

Abstract*: The flow through centrifugal impeller is highly non uniform due to formation of regions with different energy level. These region mixes at the exit of the impeller leading to loss and bringing down the efficiency of the centrifugal impeller. The present study focus on analyzing the flow through an impeller and investigating the impeller exit flows. The simulations are carried out for various mass flow rates at design and off design conditions. The velocity vectors observed depicts the regions of jet along the pressure side and wake at the suction side. The contours of total pressure and velocity depict the diffusion process that occurs within the impeller and its exit. Non uniform flow is observed along the circumferential direction of the impeller. These non uniform flow leads to secondary flow as well as loss in total pressure thereby reducing the efficiency of the centrifugal impeller.

Keywords: Centrifugal impeller, flow, exit, jet, wake, non uniform.

I. INTRODUCTION

Flow through centrifugal impellers is known to be highly complex in nature. As flow happens through centrifugal impeller, considerable distortions of flow could be visualized at exit of centrifugal impeller. Wake is observed in the suction-side-region while jet (viz., high kinetic energy fluid) is observed at the pressure-side-region. Sankaran [1] reported the study by Gallus and Subramaniam and highlighted that wake area covers up to 25% of the exit area. According to Sankaran [1] based on the work of Krain and Eckardt, the wake area covered up to thirty five percentage of exit area. The wake mass flow was around fifteen percentage of the total mass flow. Interestingly, Eckardt [2] observed this separated region extending from about 60% of the channel length to the impeller exit. Dean [3] illustrated the development of wake with detailed empirical studies of flow in an impeller. The flow left the impeller separated frequently and distorted significantly both in the meridional as well as in the circumferential plane.

Eckardt [2] reported that separated region was extending about 60% of the channel length to impeller exit. This region reduced the efficiency of the stage and diffusion within the impeller. Therefore, the intended amount of conversion of kinetic energy into static pressure was not achieved. The jet wake formation at impeller exit decreased the stage efficiency due to the additional loss caused by unsteady flow in the adjacent diffuser and mixing. The author also observed different secondary flow patterns for the shrouded and unshrouded radial impeller. The secondary flow and the tip leakage severely affected the nature of separation within the centrifugal impeller channels.

Sturge and Cumpsty [4] reported a 2D method of calculating the separated flow in centrifugal impeller. The 2D blade to blade flow was treated into two regions: jet region and wake region, separated by a free shear layer that maintained a distinct separation between these two regions. The wake region was assumed to have no flow through it. The jet flow was treated to be inviscid, irrotational, and finite difference approach was used in its solution. Eckardt [2] obtained 3D representation of the meridional velocity components between inlet and exit of the impeller at five different cross-sectional planes. These measured meridional velocity distributions portrayed the development, growth of the wake along suction side corner portion of the impeller. The circumferential velocity components were consistent and in line with the recognized fact about wake as a region of low momentum fluid.

Also, the extent of wake would be more radial if the jet coming out of the impeller was highly skewed. The meridional wakes would not mix rapidly rather than extending deep into the vaneless diffuser region. Sankaran [1] performed exit flow studies on selected centrifugal impellers. The meridional velocity distributions were observed to be smoothening out at low mass flow rates. At higher flow coefficients, a depression between two peaks was observed. Ajith Kumar [5] performed experimental investigations on exit flows on three different shrouded impellers having exit blade angles as 55 degrees, 67 degrees and 78 degrees. The increase in exit blade angle increased the operating range of the centrifugal impeller.

Soumya Dutta *et al.* [6] performed studies on impeller exit flow field through a highly loaded impeller using three holes yaw meter and hot wire anemometer.

Manuscript published on November 30, 2019.
* Correspondence Author
Seralathan S*, School of Mechanical Sciences, Department of Mechanical Engineering, Hindustan Institute of Technology and Science, Padur 603 103, Tamil Nadu, India. Email: sseralathan@hindustanuniv.ac.in
Balaji R, School of Mechanical Sciences, Hindustan Institute of Technology and Science, Padur 603 103, Tamil Nadu, India.
Mukesh Nadarajan, School of Mechanical Sciences, Hindustan Institute of Technology and Science, Padur 603 103, Tamil Nadu, India.
Ijas Ahamed A, School of Mechanical Sciences, Hindustan Institute of Technology and Science, Padur 603 103, Tamil Nadu, India.
Hariram V, School of Mechanical Sciences, Hindustan Institute of Technology and Science, Padur 603 103, Tamil Nadu, India.

The results were compared with the CFD data which revealed the difference in flow angles and turbulence intensity. Guang Xi *et al.* [7] investigated on aspect of controlling flow separation region near exit of centrifugal impeller (unshrouded type).

This separation zone, which was undesired, was controlled by increased nominal design flow rate, reducing the shroud side casing of diffuser, and reducing the shroud side blade loading. The authors observed that L2F readings of the backward curved blades gave a nearly uniform velocity profile than the radial tipped impeller. The classical "jet-wake" theory assumed an isentropic jet. The wake flow was also congruent with blade profile at exit of impeller. The authors suggested this to be corrected for any meaningful results.

McDonald *et al.* [8] analyzed the flow pattern and its variations with mass flow rate. The experimental data were compared with numerical outcomes for the flow field near centrifugal impeller exit (backward curved type). Ishida *et al.* [9] studied the velocity distribution at exit of the impeller for a varied tip clearance conditions involving two types of unshrouded centrifugal impeller. Similarly, several studies [10-19] were carried out by researchers on understanding the flow field at centrifugal impeller exit and reported ways to improve the performance of centrifugal compressor by suppressing the impact of the separation zone.

Hence, the objective of this study is to analyze the flow at exit of the shrouded centrifugal impeller. The numerical simulations are carried for three different mass flow rates, viz., m = 0.0331 kg/sec, 0.0419 kg/sec and 0.0552 kg/sec. All the numerical simulations are conducted at steady state condition.

II. NUMERICAL METHODOLOGY

The details of centrifugal compressor (low-specific speed) chosen for this investigations is illustrated in Table I.

Table-I: Operating conditions and Geometric data [1]

Pressure rise, ΔP	200 mm Water
Speed, N	1800 rpm
Outlet blade angle, β_2	65^0
Number of blade, Z	24
Blade width, b [Width at exit, b_2 is equal to at inlet, b_1]	50 mm
Inlet blade angle, β_1	35^0
Diameter at impeller exit, d_2	550 mm
Diameter at impeller entry, d_1	280 mm
Diameter ratio, d_1/d_2	0.51
Mass flow rate, m	1.003 kg/s

As experimental data [1] is on hand, the same is chosen to model and investigate numerically. Geometric model deployed for simulation consists of a shrouded impeller with blade. On the basis that flow is periodic in impeller's blade passages, the concept of single passage approach (i.e., one blade passage) is deployed to model the configuration instead of modeling the entire impeller geometry. This approach saves enormous computational resources and time. The point by point method is adopted to design the impeller blade using ANSYS ICEMCFD [18, 19]. The inlet of fluid domain is kept at the forefront by a measurement of half the blade chord length whereas the domain's exit is placed at a distance of $1/4^{th}$ of blade's chord length. During meshing, unstructured grid is generated using tetrahedral elements for the entire computational domain. At least six fine prism shaped cell are deployed nearer to wall to facilitate better resolution within the boundary layer as illustrated in Fig. 1. ANSYS ICEMCFD is utilized to perform modeling and meshing of fluid domain.

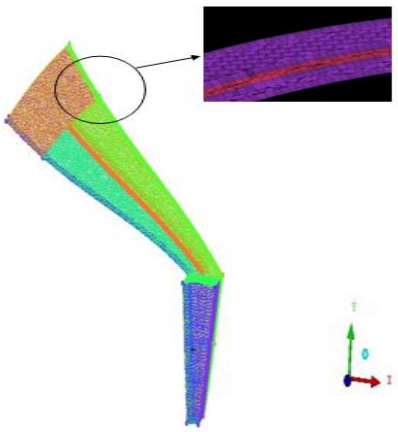

Fig. 1. Unstructed mesh

Table-II: Details of grid independency

Element count	Energy coefficient, ψ	
	Standard kω	*kω shear stress transport (SST)*
397471	0.948	0.9894
500961	0.967	1.028
776868	1.001	1.061

Table-III: Turbulence model study

Flow coefficient, $\Phi = C_m/U$	Mass flow rate (kg/s)	Energy coefficient, ψ		
		Turbulence models		Expt. [1]
		Standard kω	*kω shear stress transport (SST)*	
0.19 (design)	0.04198	1.001	1.061	1.08

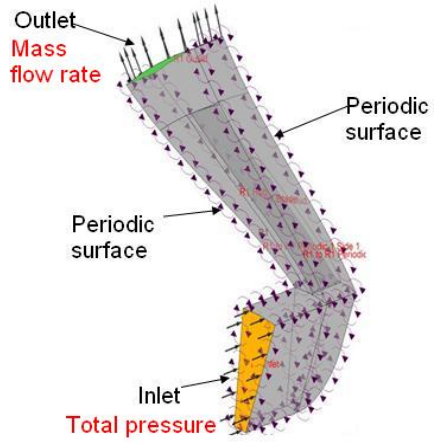

Fig. 2. Boundary conditions

Table II list the grid independency test details carried out for mass flow rate, m = 0.0419 kg/s. This is done to ensure independency of the result irrespective of mesh generated. Based on these, the element count (prism and tetrahedral) in the fluid domain is 776868 elements.

Two equation models namely, kω SST and standard kω turbulence model is utilized to perform turbulence model study. These details are listed in Table III. The obtained data are verified with the experimental result [1].

Since data based on kω SST model is closer, further studies are performed using kω SST turbulence model [18, 19].

Figure 2 depicts definition of each boundary. Computational domain inlet is placed 105 mm ahead from eye of the impeller. This approach ensures that inlet boundary conditions aren't impaired by the back pressure created by impeller. Rotating frame of reference is specified for the entire domain. Total pressure in stationary frame is the inlet boundary condition in which reference pressure mentioned is 101.325 kN/m^2. As a result, at inlet, zero Pa is the relative total pressure. The fluid mentioned is air at 25^{0}C. kω SST turbulence model is chosen owing to its accuracy and robustness, and turbulence intensity is mentioned to be 1% (with medium level). Rotational periodic boundary is mentioned for the side walls of impeller domain. The outlet is mentioned as mass flow rate. The impeller is rotating with an angular velocity same as the domain. With reference to relative reference frame, it's stationary and it is mentioned with wall boundary conditions. The wall is mentioned as no-slip. Roughness of wall is ignored and it is assumed to be smoother. Simulations are executed with FVM based CFD code, ANSYS CFX. The governing equations are resolved under steady state solutions till the residuals got converged. The target variable monitored at impeller outlet is mass averaged pressure. The RMS residuals convergence conditions of all governing equations are set as 10^{-4} [18, 19].

III. RESULTS AND DISCUSSION

The numerical investigation outcomes for mass flow rate m = 0.0331 kg/sec, 0.0419 kg/sec and 0.0552 kg/sec at off-design and design conditions are discussed. Turbo surface is introduced to elucidate the flow physics of flow within the impeller. It is introduced at five axial locations namely 16%, 33%, 55%, 66% and 81% between shroud and hub along axial plane in-line with impeller width.

The stagnation pressure distribution at impeller exit is illustrated in Figures 3, 4, and 5 for mass flow rate m = 0.0331 kg/sec, 0.0419 kg/sec and 0.0552 kg/sec respectively. The diffusion occurs due to increase in radius / area which result in conversion of angular momentum into rise in static pressure. Diffusion occurs due to increase in flow passage area which results in conversion of the angular momentum into rise in static pressure. Total pressure rises with increase in radius ratios which is reflected in various mass flow rates.

Figure 6 illustrates the total pressure distributions across the span for various mass flow rates. The stagnation pressure distribution is observed to be slightly higher near the hub side. This similarity in the trend is observed for all mass flow rates. Similarly, the stagnation pressure distribution increases with mass flow rates.

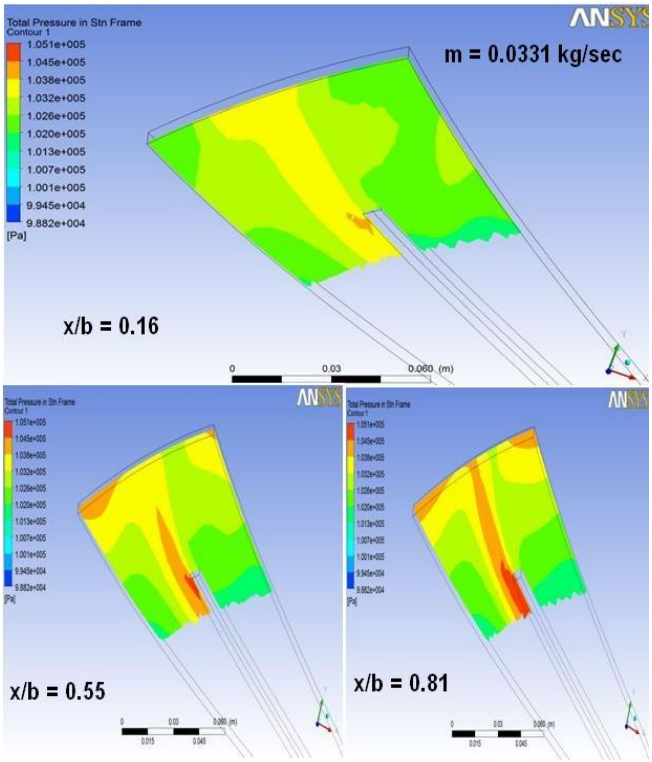

Fig. 3. Stagnation pressure distribution; m = 0.0331 kg/s

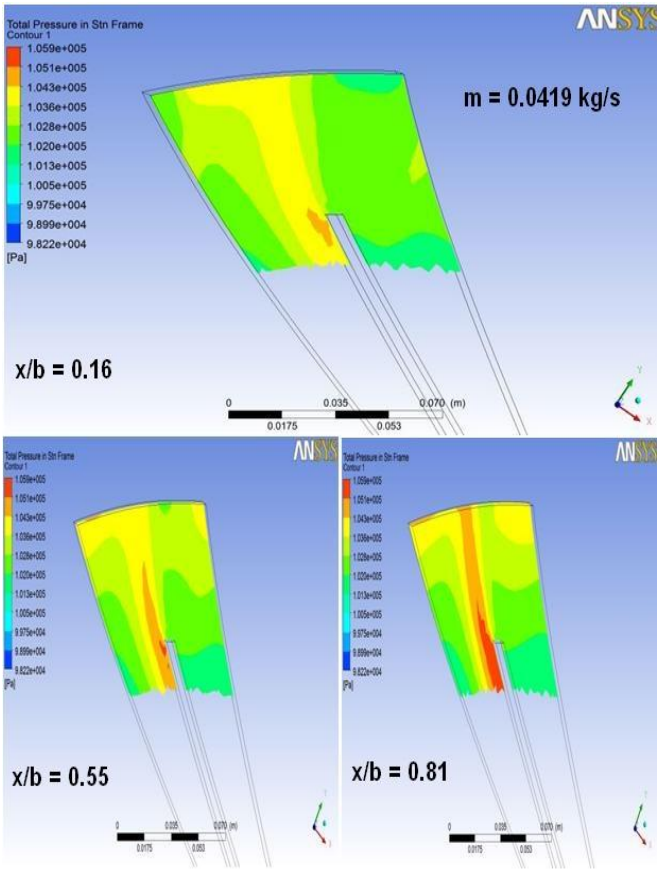

Fig. 4. Stagnation pressure distribution; m = 0.0419 kg/s

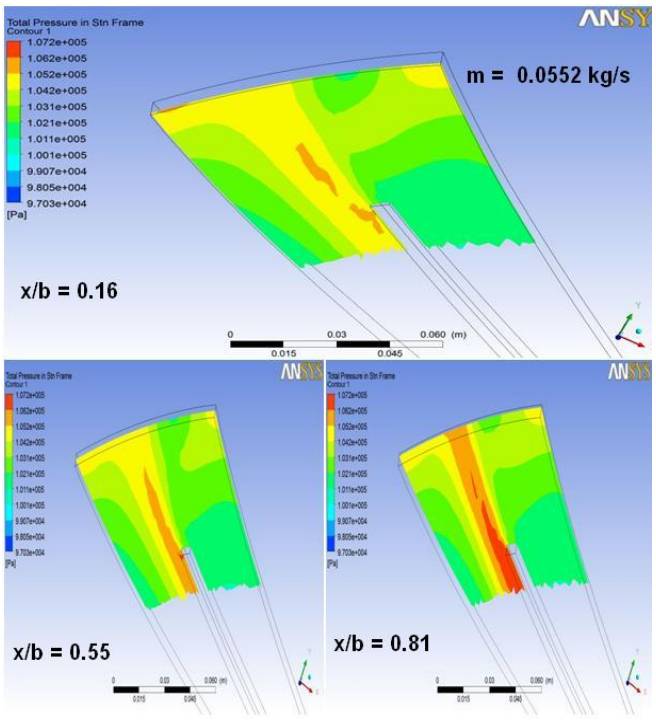

Fig. 5. Stagnation pressure distribution; m = 0.0552 kg/s

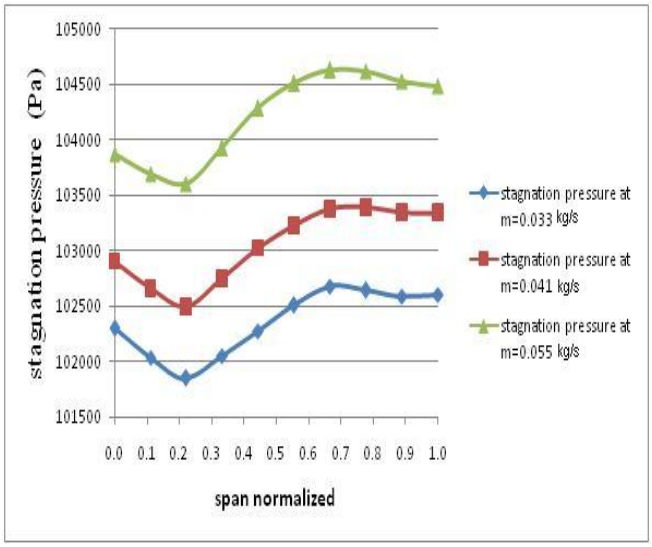

Fig. 6. Stagnation pressure distributions at impeller exit

Figures 7, 8, and 9 illustrates the velocity distribution at impeller exit for various mass flow rate namely for mass flow rates m = 0.0331 kg/sec, 0.0419 kg/sec and 0.0552 kg/sec respectively. As radius ratio increases along with increase in area of the flow passage, velocity decreases. The velocities nearer the hub are observed to be slightly higher for various mass flow rates.

Similarly, non uniformity in the flow is observed at the impeller exit. The region of higher energy level (jet) and region of lower energy level (wake) could be clearly observed as flow occurs through the impeller and at the impeller exit. This leads to mixing of different energy level leading to loss in stagnation pressure and thus reducing the efficiency of the centrifugal compressor. Also, the flow is observed to be non uniform in both circumferential as well in axial directions.

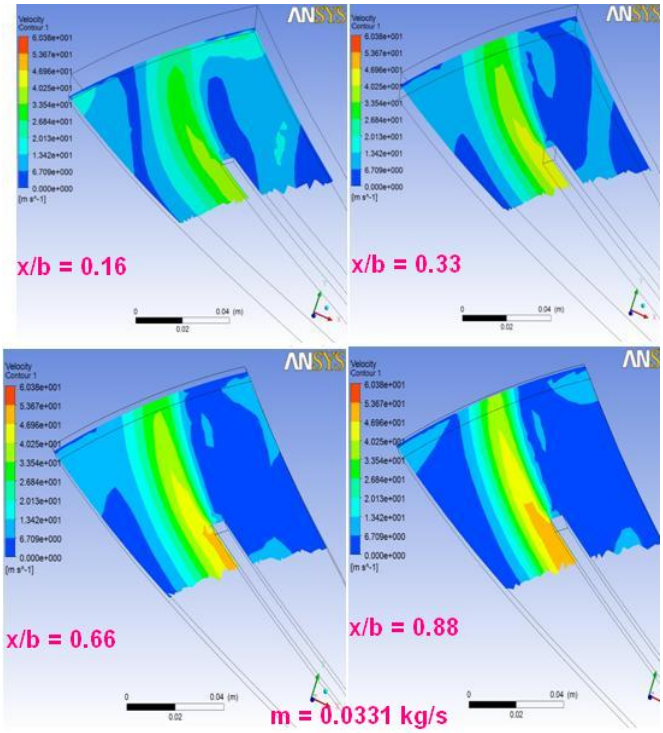

Fig. 7. Velocity distribution; m = 0.0331 kg/s

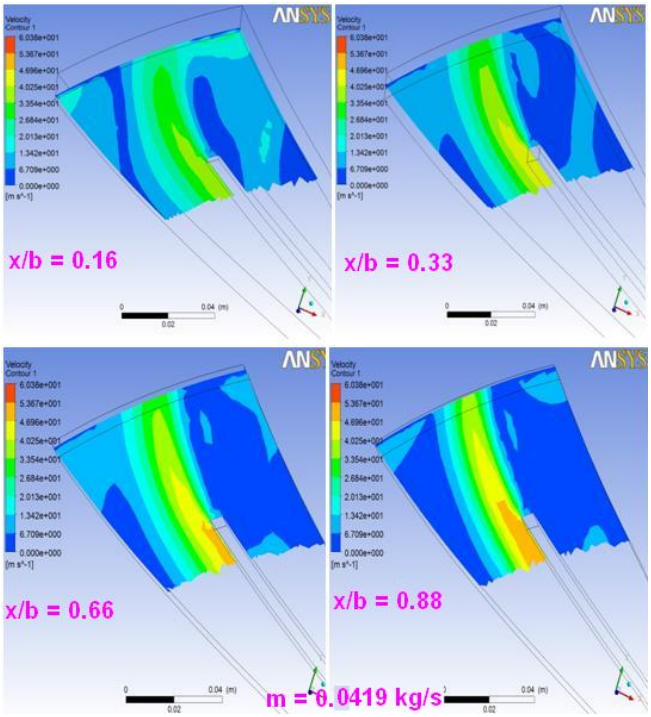

Fig. 8. Velocity distribution; m = 0.0419 kg/s

Figure 10 illustrates the velocity distribution for various mass flow rates. The velocity observed nearer the hub is slightly higher compared to shroud side for different mass flow rates. Similarly, non uniformity in the flow is observed at the impeller exit.

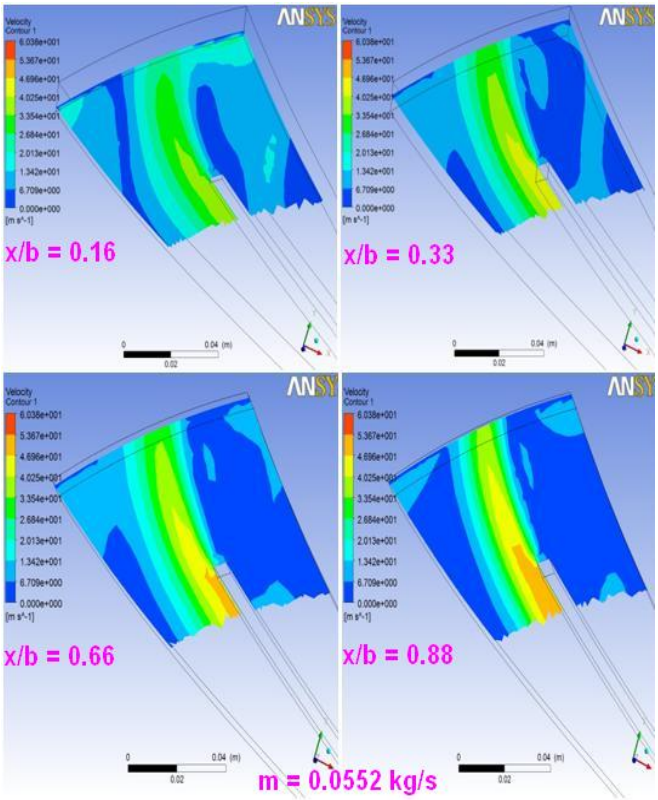

Fig. 9. Velocity distributions; m = 0.0552 kg/s

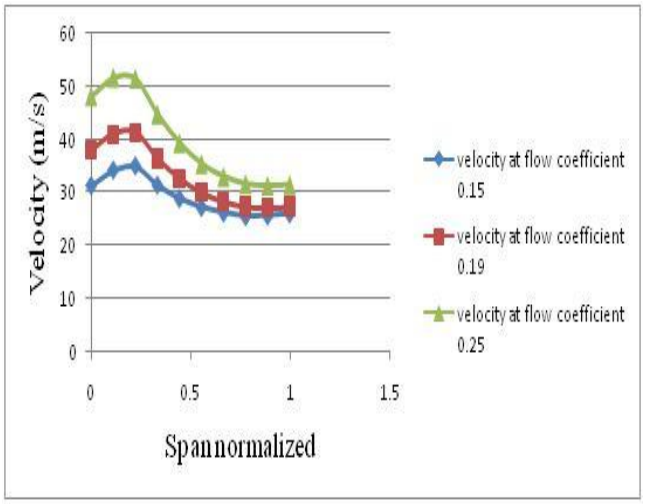

Fig. 10 Velocity distribution at impeller exit

Figure 11 depicts the velocity vectors for various mass flow rates. As can be seen in the Figures, the region of high velocity region (jet) as well as region of low energy region (wake) can be visibly observed. These regions possessing dissimilar energy level lead to non uniform flow all along circumferential direction. These non uniformity leads to mixing of fluids with different energy levels which may not occur instantaneously at the impeller exit but takes place in the vaneless diffuser region. This brings down the efficiency of the centrifugal impeller as the increased total pressure losses.

The velocity distribution at meridional plane is shown in Figure 12. Velocity reduces gradually from impeller inlet to its exit. The meridional velocity distribution is uniform for mass flow rates m = 0.0331 kg/sec and 0.0419 kg/sec. At mass flow rate m = 0.0552 kg/sec, the flow separation is observed near the hub wall.

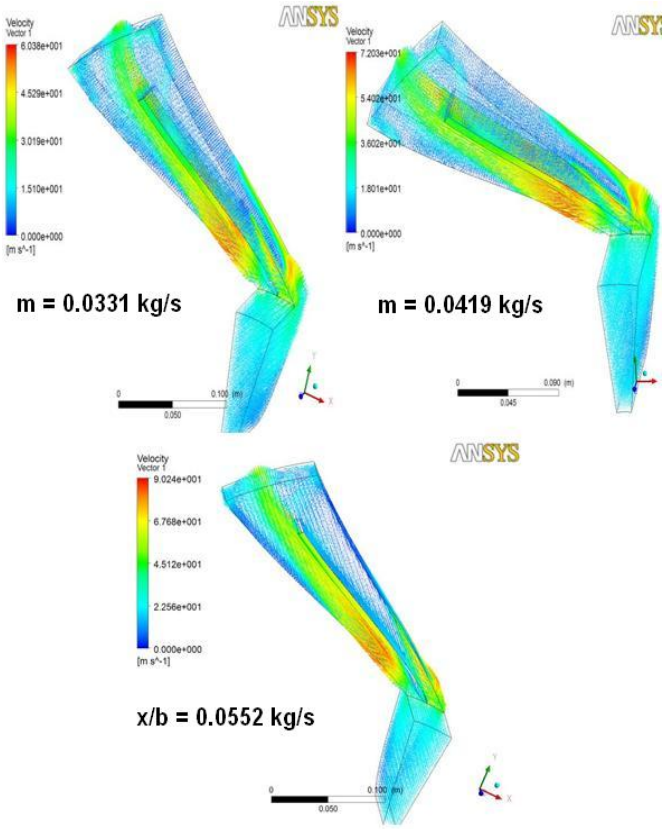

Fig. 11 Jet and wake formation

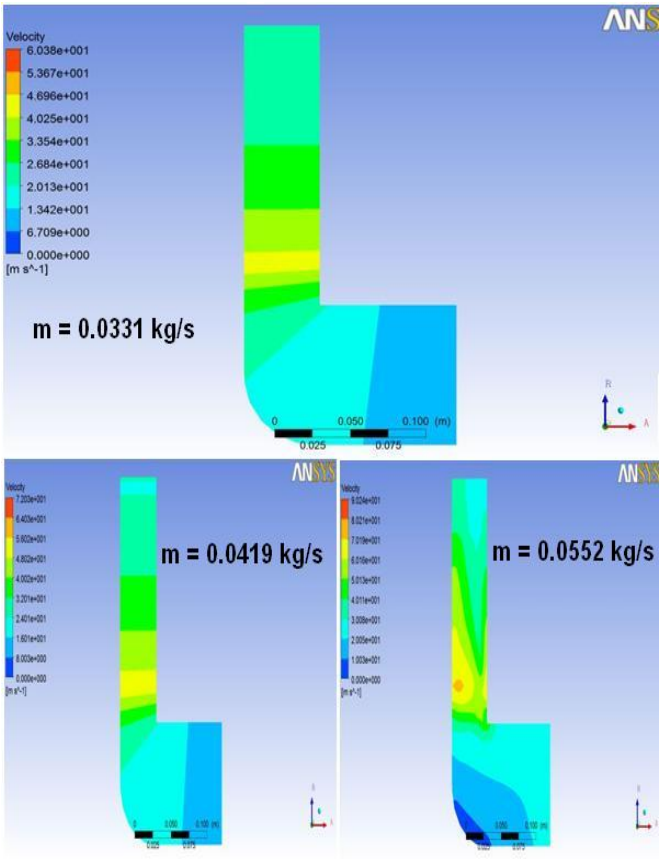

Fig. 12. Velocity distribution in meridional plane

Studies of the previous works on flow phenomena of centrifugal impellers indicate the accumulation of low energy fluid (wake) along the shroud-suction side corner of the impeller blade channel which leads in most cases of the highly loaded impellers to more or less pronounced flow separation. Similar pattern is also observed in this present study. This flow separation impairs the diffusion potential and leads to a highly distorted jet-wake velocity pattern at impeller exit.

The mixing loss is also directly dependent on the magnitude of the wake flow, which is a function of wake flow area. Therefore, larger the wake flow fraction, more mixing will take place between the jet and wake flows and larger the mixing loss will be.

Also, it leads to a significant decrease in total pressure at diffuser inlet. This is due to intensive jet-wake mixing at downstream of the impeller and because of higher velocities, resulting in higher frictional losses. As the flow passes through the diffuser, the flow becomes homogenous, so friction and separation losses dominate. Also, at off-design conditions, the jet-wake mixing strongly affects the total pressure loss.

IV. CONCLUSION

Numerical simulations are performed for the flow through the centrifugal impeller and the nature of flow at impeller exit is investigated for various mass flow rates at design and off-design conditions. Based on the study, the following observations are made.

- As the area increases, diffusion occurs within the centrifugal impeller leading to increase in static and total pressure.
- Total pressure gradually increases from impeller entry to exit
- Increase in static pressure is observed to be gradual from impeller inlet to its exit.
- Region of higher energy level (jet) and region of lower energy level (wake) is clearly observed as flow occurs within the impeller passage and its exit.
- Flow is observed to be non uniform along the circumferential direction.
- Mixing occurs due to fluid with different energy level leading to total pressure loss.

ACKNOWLEDGMENT

The authors would like to acknowledge the support provided by the CAD Laboratory, Department of Mechanical Engineering, HITS, Padur, Tamil Nadu in carrying out this study.

REFERENCES

1. K. Sankaran, “Flow studies at the exit of centrifugal impellers,” Ph. D., Thesis, Department of Mechanical Engineering, IIT Madras, Chennai, 1985.
2. D. Eckardt, “Detailed flow investigations within a high-speed centrifugal compressor impeller,” ASME Journal of Fluids Engineering, vol. 98 (3), 1976, pp. 390-399.
3. R. C. Dean, “The fluid dynamic design of advanced centrifugal compressor’s,” Technical Note TN-185.
4. D. P. Sturge and N. A. Cumpsty, “Two dimensional method for calculating separated flow in a centrifugal impeller,” ASME Journal of Fluids Engineering, vol. 97, 1975, pp. 581-597.
5. R. Ajith Kumar, “Exit flow studies on some centrifugal impellers,” M. Tech Thesis, Department of Mechanical Engineering, IIT Madras, Chennai, 1990.
6. Soumya Dutta, Wataru Sato, Kenchi Funazaki, and Yukiya Kakudate, “Investigation of impeller exit flow field in a highly loaded centrifugal compressor,” ASME Paper No. AJKFluids2015-2745, V001T02A003, 2015, 6 pages.
7. Guang Xi, Xuechen Li, and Wuqi Gong, “Study on the controlling of flow separation zone near unshrouded impeller exit for centrifugal compressors,” ASME Paper No. GT2013-94792, V06CT40A007, 2013, 8 pages.
8. G. B. McDonald, E. Lennemann, and J. H. G. Howard, “Measured and predicted flow near the exit of a radial-flow impeller,” vol. 93, Issue 4, 1971, pp. 441-446.
9. M. Ishida, Y. Senoo, and H. Ueki, “Secondary flow due to the tip clearance at the exit of centrifugal impellers,” ASME Journal of Turbomachinery, vol. 112, Issue 1, 1990, pp. 19-24.
10. Jong Sik Oh, “Numerical investigation of internal flow field for modified design of Eckardt backswept impeller,” ASME Paper No. 98-GT-296, V001T01A081, 1998, 10 pages.
11. H. Venkatesan, J. J. Godwin, and S. Sivamani, “Data set for extraction and transesterification of bio-oil from Stoechospermum marginatum, a brown marine algae,” Data in Brief, vol. 14, 2017, pp. 623-628.
12. P. T. Micha, T. Mohan, and S. Sivamani, “Design and Analysis of a Permanent Magnetic Bearing for Vertical Axis Small Wind Turbine,” Energy Procedia, vol. 117, 2017, pp. 291-298.
13. V. Hariram, J. G. John, and S. Seralathan, “Spectrometric analysis of algal biodiesel as a fuel derived through base-catalysed transesterification,” International Journal of Ambient Energy, vol. 40, Issue 2, 2019, pp. 195-202.
14. S. Seralathan, and D. G. Roy Chowdhury, “Performance enhancement of a low-pressure ratio centrifugal compressor stage with a rotating vaneless diffuser by impeller disk extended shrouds,” Journal of Applied Fluid Mechanics, vol. 9, Issue 8, 2016, pp. 2933-2947.
15. H. Venkatesan, G. John, and S. Sivamani, “Cotton seed biodiesel as alternative fuel: Production and its characterization analysis using spectroscopic studies,” International Journal of Renewable Energy Research, vol. 7, Issue 3, 2017, pp. 1333-1339.
16. G. John, V. Hariram, and S. Seralathan, “Emission reduction using improved fuel properties of algal oil biodiesel and its blends,” Energy Sources, Part A: Recovery, Utilization and Environmental Effects, vol. 40, Issue 1, 2018, pp. 45-53.
17. V. Hariram, S. Seralathan, K. M. Dinesh, S. Vasanthaseelan, M. Sabareesh, “Analyzing the fatty acid methyl esters profile of palm kernel biodiesel using GC/MS, NMR and FTIR techniques,” Journal of Chemical and Pharmaceutical Sciences, vol. 9, Issue 4, 2016, pp.122-3128.
18. M. Govardhan and S. Seralathan, “Effect of forced rotating vaneless diffusers on centrifugal compressor stage performance,” Journal of Engineering Science and Technology, vol. 6, Issue 5, October 2011, pp. 562-578.
19. S. Seralathan, and D. G. Roy Chowdhury, “Modification of centrifugal impeller and effect of impeller extended shrouds on centrifugal compressor performance,” Procedia Engineering, vol. 64, 2013, pp. 1119-1128.